GPS MULTIPATH REDUCTION WITH CORRELATOR BEAMFORMING

THESIS

Jason M. Barhorst, Captain, USAF

AFIT-ENG-14-M-10

DEPARTMENT OF THE AIR FORCE
AIR UNIVERSITY

AIR FORCE INSTITUTE OF TECHNOLOGY

Wright-Patterson Air Force Base, Ohio

AFIT-ENG-14-M-10

GPS MULTIPATH REDUCTION WITH CORRELATOR BEAMFORMING

THESIS

Presented to the Faculty

Department of Electrical and Computer Engineering

Graduate School of Engineering and Management

Air Force Institute of Technology

Air University

Air Education and Training Command

in Partial Fulfillment of the Requirements for the

Degree of Master of Science in Electrical Engineering

Jason M. Barhorst, B.S.

Captain, USAF

March 2014

AFIT-ENG-14-M-10

GPS MULTIPATH REDUCTION WITH CORRELATOR BEAMFORMING

Jason M. Barhorst, B.S.
Captain, USAF

Approved:

//signed//	14 March 2014
Dr. John F. Raquet (Chairman)	Date
//signed//	14 March 2014
Dr. Peter J. Collins (Member)	Date
//signed//	14 March 2014
Maj Marshall E. Haker (Member)	Date

AFIT-ENG-14-M-10

Abstract

This research effort investigates the feasibility of beamforming using a single Global Positioning System (GPS) front end. Traditional methods of beamforming use multiple front ends, typically one per antenna element. By enabling a receiver to sample a switched antenna array, the hardware cost of implementing a GPS antenna array can be significantly reduced. Similar techniques of reducing the number of receivers have been used by Locata Corporation in the design of their non-GPS positioning systems. However, Locata Corporation's local transmitters provide a signal strength much higher than GPS's signal strength. For this reason, the inclusion of low-noise amplifiers into the GPS based system was investigated.

GPS data was collected using a multiple channel antenna array. Simulated switching was then performed to combine the four channels of data in to a single channel of switched data. Next, a GPS receiver using correlator beamforming was developed to apply the necessary phase shift to each data sample and form an antenna beam in the direction of the desired satellite. The switched data was processed and analyzed with the receiver. The results successfully demonstrated the potential for correlator beamforming to be used with GPS signals. Additional experiments were performed with simulated GPS data to further characterize the capability of the receiver.

Acknowledgements

I want the thank my wife and children for providing me with the motivation to seek higher education. I would also like to thank all the professors at AFIT's Department of Electrical and Computer Engineering. In particular, I want to thank my advisor Dr. Raquet. With out his guidance, patience, and persistence, I never would have completed my studies. Finally, I'd like to express my thanks and appreciation to Locata Corporation for sponsoring this research and providing heaps of invaluable information about their technology.

Jason M. Barhorst

Table of Contents

Page

List of Figures

List of Tables

GPS MULTIPATH REDUCTION WITH CORRELATOR BEAMFORMING

I. Introduction

A significant issue with GPS is the existence of multipath. Multipath results from the GPS signal arriving at the antenna location via indirect means (e.g. reflecting off a building). This affects the GPS receiver's ability to track the correlation peak, resulting in position errors [12].

One technique of reducing the impact of multipath is using a phased antenna array. Such an antenna array is capable of introducing a phase shift to each element of said array, thereby steering a beam in the direction of the desired signal. Traditionally, these beamforming antenna arrays require an RF front end for each antenna, which makes them relatively expensive. Generally, to form tighter (more narrow) beams, an antenna array will require more elements. With the addition of more elements, cost can increase to unreasonable amounts.

With correlator beamforming, a single front end can be used with a hardware switched antenna array. The cost savings of using a single front end continues to improve as additional elements are desired, when compared to the cost of using multiple front ends. Currently, Locata is operating an 80 element Orb antenna with a single channel receiver [11].

1.1 Research Objectives

Locata has developed the use of correlator beamforming with local positioning systems. This local positioning system makes use of local signal transmitters, "LocataLites," to transmit ranging signals similar to those used by GPS [4]. However,

the use of LocataLites allows for a much stronger signal to be transmitted. With GPS, the signal is much weaker, well below the noise floor [9]. For this reason, there was some uncertainty that correlator beamforming would be practical with GPS.

The weak signal of GPS requires that low-noise amplifiers (LNAs) be placed between the antenna element and receiver. Typically, the LNAs are located as close to the antenna as practical. One concern with the introduction of LNAs was that they have not previously been used with correlator beamforming. It was uncertain if the LNAs would be phase coherent (each LNA introducing the same effect on path length). Additionally, the LNAs may not be phase stable (phase delay may drift or vary with environmental conditions).

The objective research effort was to determine if correlator beamforming is compatible with the GPS signal. Through the use of both real and simulated data, the feasibility of correlator beamforming with GPS signals was investigated. Additional efforts were made to determine if the presence of LNAs presented any challenges or limitations to beamforming.

1.2 Thesis Overview

Chapter II begins with an introduction to GPS navigation, including motivation, calculating position and timing solutions, signal structure, and receiver algorithms. The next section discusses the basics of antenna arrays and how directional beamformimg can be accomplished by applying specific phase shifts to each antenna element. Finally, Locata's method of correlator beamforming is discussed and applied to the GPS receiver algorithm.

Chapter III covers the methodology necessary to perform experiments and obtain results. The chapter begins with data collection using a multiple channel GPS receiver. After collection, the data was combined to simulate antenna switching. Next,

a simulated GPS signal generator was developed to allow for testing specific satellite and multipath scenarios. Finally, the GPS correlator beamforming receiver design and implementation is discussed.

Chapter IV starts by presenting the results of the four channel collected real GPS data. To validate the GPS signal simulator, test data was produced to closely mimic the collected data. After validation, the signal simulator was used to test the correlator beamforming receiver's ability to create an antenna beam and reject multipath.

The final chapter, Chapter V, presents the conclusions and significance of the research effort. Finally, guidance is provided for anyone who continues this research effort by providing recommendations for the way forward.

II. Background

2.1 Chapter Overview

This chapter introduces the fundamentals of the Global Positioning System (GPS) and antenna arrays necessary to understand correlator beamforming. Locata Corporation's technique of correlator beamforming will be then be discussed.

2.2 Fundamentals of GPS

The Global Positioning System provides a means for users to have access to accurate position, velocity, and time solutions. This position/timing solution is obtained by receiving the broadcast GPS signals with an antenna and processing the received signals with a GPS receiver. The addition of multipath, due to reflected signals, can reduce the accuracy of the GPS position/timing solution. Each of these topics is covered in greater detail below.

2.2.1 Obtaining a Position Solution.

The following pseudorange equation is the foundation for calculating a GPS position and timing solution:

$$\rho_c^{(k)} = \sqrt{(x^{(k)} - x)^2 + (y^{(k)} - y)^2 + (z^{(k)} - z)^2} + c \cdot \delta t + \varepsilon_\rho^{(k)} \tag{1}$$

where $\rho_c^{(k)}$ is the pseudorange estimated by the GPS receiver, $(x^{(k)}, y^{(k)}, z^{(k)})$ is the Earth-Centered Earth-Fixed (ECEF) coordinate location of the k^{th} satellite, (x, y, z) is the ECEF receiver location, c is the speed of light, δt is the receiver clock error, and $\varepsilon_\rho^{(k)}$ represents the residual errors of the k^{th} pseudorange [9].

In Equation (1) the pseudorange ($\rho_c^{(k)}$) is measured by the GPS receiver, the

satellite position $(x^{(k)}, y^{(k)}, z^{(k)})$ is included in the ephemeris data transmitted by the GPS satellite, and the speed of light, c, is constant. This results in an equation with four unknowns, the receiver position (x, y, z) and the receiver clock error (δt). To solve for all unknowns, the GPS receiver must track a minimum of four satellites $(k = 1, 2, 3, 4)$. Assuming exactly four satellites are being tracked, this provides a system of four equations with four unknowns because the receiver position and clock error are common to all four pseudoranges.

$$\rho_c^{(1)} = \sqrt{(x^{(1)} - x)^2 + (y^{(1)} - y)^2 + (z^{(1)} - z)^2} + c \cdot \delta t + \varepsilon_\rho^{(1)}$$

$$\rho_c^{(2)} = \sqrt{(x^{(2)} - x)^2 + (y^{(2)} - y)^2 + (z^{(2)} - z)^2} + c \cdot \delta t + \varepsilon_\rho^{(2)}$$

$$\rho_c^{(3)} = \sqrt{(x^{(3)} - x)^2 + (y^{(3)} - y)^2 + (z^{(3)} - z)^2} + c \cdot \delta t + \varepsilon_\rho^{(3)}$$

$$\rho_c^{(4)} = \sqrt{(x^{(4)} - x)^2 + (y^{(4)} - y)^2 + (z^{(4)} - z)^2} + c \cdot \delta t + \varepsilon_\rho^{(4)}$$

This system of four non-linear equations with four unknowns can be solved in a variety of ways. Once solved, the receiver position and clock error are both known. The clock error can be used to adjust the receiver clock if accurate timing is required.

2.2.2 Signal Structure.

The GPS L1 signal structure is composed of several parts as shown in Equation (2):

$$s(t) = A_{P_{L1}} Y(t) N(t) cos(2\pi f_{L1} t) + A_{C/A} CA(t) N(t) cos(2\pi f_{L1} t) \tag{2}$$

where $s(t)$ is the total signal, $A_{P_{L1}}$ is the amplitude of the L1 P-code signal, $Y(t)$ is the P-code, $N(t)$ is the navigation message, f_{L1} is the frequency of the L1 carrier signal, $A_{C/A}$ is the amplitude of the C/A-code signal, and $CA(t)$ is the C/A-code [9].

The C/A-code is of particular importance in this research effort. The C/A-code is

a pseudorandom series of chips (+/- 1) unique to each satellite PRN. This allows the GPS receiver to distinguish between and track multiple satellites at the same time. This is necessary for calculation of the position solution. Locking onto the C/A-code is typically performed using a correlation function, a process that multipath tends to degrade. For that reason, multipath reduction can improve the accuracy of the C/A-code tracking, thus improving the accuracy of the pseudorange calculations.

2.2.3 GPS Receiver Algorithm (tracking loops).

The basic algorithm for a GPS receiver is shown in Figure 1. Of particular importance to correlator beamforming is the Doppler removal portion, which uses the reference carrier ϕ_{ref_k}.

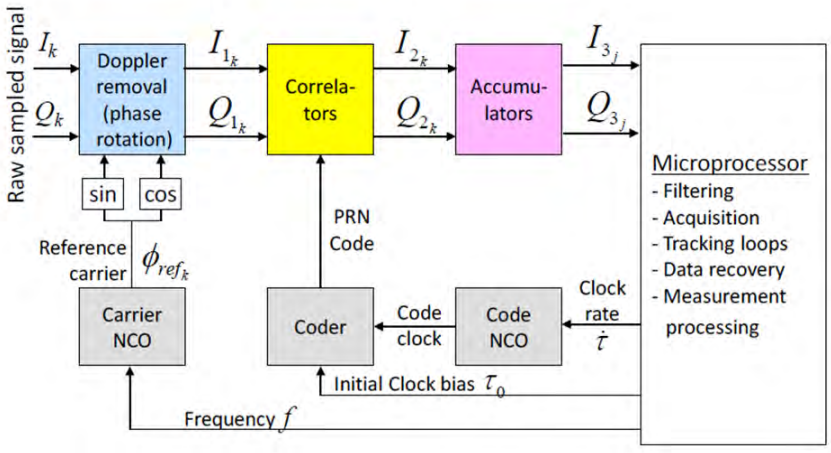

Figure 1. GPS Receiver Algorithm (Figure provided by [10])

The reference carrier phase is the value that is augmented with beamforming phases to perform correlator beamforming.

2.3 Antenna Arrays and Beamforming

2.3.1 Basic Arrays.

According to [3], there are a minimum of five factors which can be used to control the radiation pattern of an antenna array:

1. Array Geometry (linear, circular, etc.)
2. Element Spacing
3. Amplitude/Gain of Relative Elements
4. Phase of Relative Elements
5. Pattern of Individual Elements

Typically, items 1, 2, and 5 are fixed for a given antenna array, as is the case in this thesis. The amplitudes for each of the elements was assumed to be the same, so no gain adjustments were made in this effort. The antenna pattern manipulation for this effort was conducted by adjusting the phase of relative antenna elements.

2.3.2 Phased Array.

For the purpose of this thesis, the focus was on adjusting the phase of the elements to create an antenna beam in the direction of the desired signal, commonly referred to as adaptive or direction-of-arrival algorithms for smart-antennas [3]. This technique can ensure maximum antenna gain in the direction of the desired signal. Assuming the location of the antenna elements and source of the desired signal are known, the beamforming phases can be calculated using the path length difference between the relative signals. Figure 2 shows the scenario where the range between each antenna element and the signal's source is known. Using that information, the necessary beamforming phases can be calculated as follows [3]:

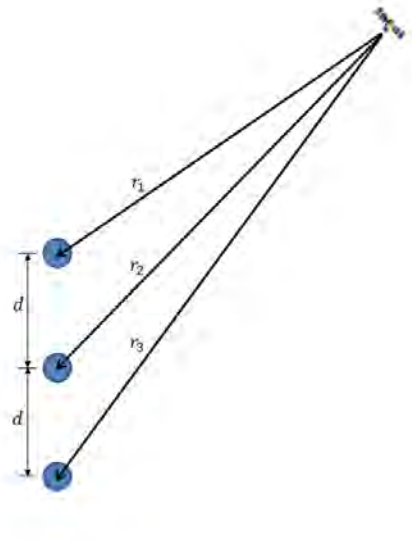

Figure 2. Signal Path Length

$$\phi_{BF_{12}} = \frac{r_1 - r_2}{\lambda} \tag{3}$$

$$\phi_{BF_{32}} = \frac{r_3 - r_2}{\lambda} \tag{4}$$

where ϕ_{BF} is the beamforming phase in cycles, r_1 is the range from the satellite to the first antenna element, r_2 is the range from the satellite to the second antenna element, r_3 is the range from the satellite to the third antenna element, and λ is the signal's wavelength. Equations (3) and (4) calculate the phase shift necessary to bring the signal at antenna element 1 and 3 in phase with the signal at element 2, respectively. This technique ensure that the signal from the satellite can be constructively combined by applying the appropriate phase shift and summing.

For this research effort all processing was done after data collection (post-processed) or on simulated data. As such, the location of the antenna elements and satellites was always know, and allowed for beamforming phases to be calculated as described above. Often, the location of the antennas and signal source is not explicitly known, but a general signal Angle of Arrival (AoA) is desired. This scenario is shown in Fig-

ure 3. Given the desired AoA, the beamforming phase can be approximated based

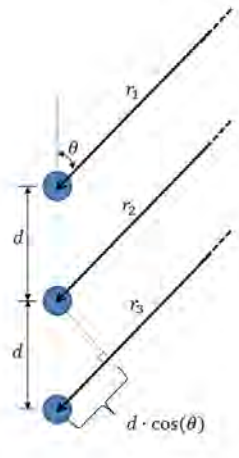

Figure 3. Signal Angel of Arrival

on antenna geometry. This technique assumes the source is sufficiently far away from the antenna that the signals arriving at each antenna are traveling approximately parallel with each other. In the case of the simple linear array shown in Figure 3, the beamforming phases are:

$$\phi_{BF_{12}} = -\frac{dcos(\theta)}{\lambda} \tag{5}$$

$$\phi_{BF_{32}} = \frac{dcos(\theta)}{\lambda} \tag{6}$$

where ϕ_{BF} is the beamforming phase in cycles, d is the element spacing, θ is the AoA of the desired signal, and λ is the signal's wavelength.. Equations (5) and (6) approximate the phase shift necessary to bring the signal at antenna element 1 and 3 in phase with the signal at element 2, respectively.

Beamforming also provides some reduction of undesired signals (multipath), depending on the angle of arrival of the multipath. If the multipath arrives from the direction of a small (low gain) side lobe or null, then the majority of the multipath signal will be rejected. However, if the multipath signal arrives from approximately

the same direction as the desired signal, then the rejection will be much less, depending on the beam width. This possibility for arrival of an undesired signal often leads to larger arrays, with more antenna elements to create narrower beams, thus reducing the chance of receiving an undesired signal. This is the perfect situation for correlator beamforming since additional antenna elements can be used without significantly increasing the cost.

2.4 Correlator Beamforming

Locata Corporation has been able to design switched antenna arrays that utilize multiple antenna elements with a single RF front end. These antenna arrays are designed to work with their LocataLites (LocLites). LocLites are transceivers used to produce accurate range measurements. The LocLites are similar in nature to GPS satellites, but operate at a higher frequency and power [4]. This higher operating power allows for antenna arrays to be built without in-line signal amplifiers. The requirement for low-noise amplifiers in the design of a switching GPS antenna is one of the primary concerns that will be addressed by this research effort.

2.4.1 Implementation of Correlator Beamforming in a GPS Receiver.

The beamforming is performed by switching though every antenna element within a single integration period, and then combining the individual samples with the appropriate phase shift applied. Figure 4 shows how the traditional GPS receiver was modified to perform correlator beamforming. Note that the receiver shown in Figure 4 assumes that multiple RF front ends are used to collect the data, and the switching occurs in post-processing. In a real world receiver, the antenna would be physically switched with a series of RF switches and a single RF front end would downconvert the switched data.

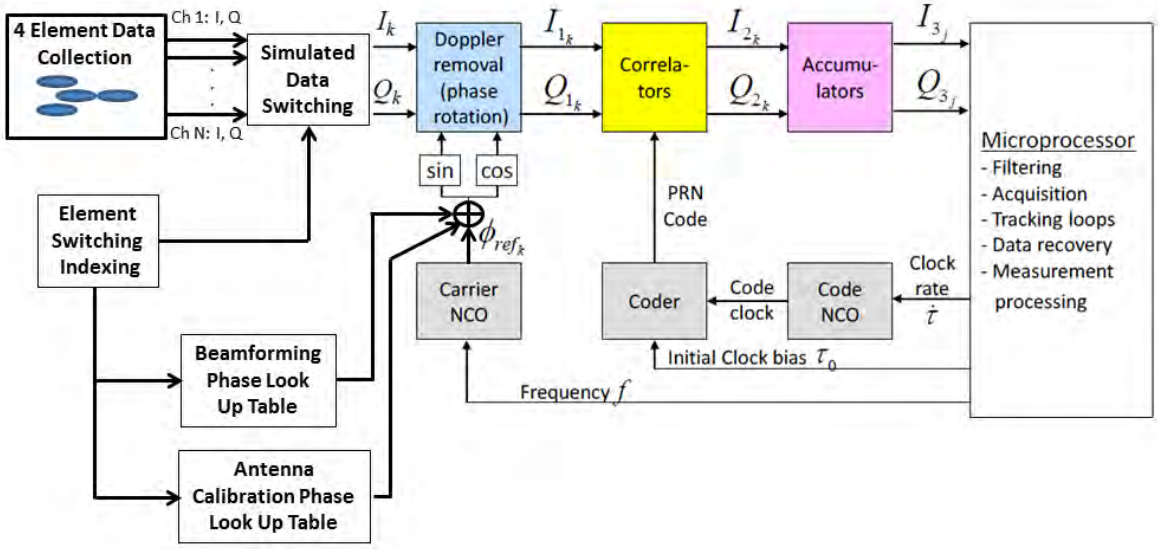

Figure 4. GPS Receiver Algorithm with Beamforming

2.5 Summary

This section provided an introduction to GPS navigation. Antenna arrays were briefly discussed, with emphasis on applications to correlator beamforming. The methods used by Locata Corporation were covered and the top level view of the modified GPS receiver algorithm capable of performing correlator beamforming was presented.

III. Methodology

3.1 Chapter Overview

This chapter will present the techniques used to evaluate correlator beamforming applications for GPS. The process began by using a four channel receiver connected to a four element antenna array. This configuration allowed for synchronous sampling of four channels. These four synchronized data collections were critical to calibrating the antenna and demonstrating correlator beamforming capability with real world GPS data. Additional data sets were generated using a signal simulator written in MATLAB®. These simulated data sets allowed for the testing of a variety of GPS satellite, multipath, and antenna array configurations.

With the ability to beamform using both real and simulated data sets, it was necessary to investigate potential hardware issues facing physical implementation of a switched GPS antenna array. Specifically, the LNAs were under question. Locata Corporation's antenna arrays do not incorporate LNAs because of the stronger signals used in their local positioning systems. The unknown phase stability properties of the LNAs were of particular concern. For this reason, two different types of LNAs were bench tested for phase start-up repeatability, drift, and temperature variation.

3.2 GPS Receiver, Antenna Array, and Data Collection

3.2.1 GPS Receiver.

The sample data was collected on the Transform-Domain Instrumentation Global Navigation Satellite System Receiver (TRIGR), a multiple channel receiver designed at Ohio University. The TRIGR is capable of coherently sampling multiple channels of navigation data, on a variety of signals and frequencies (GPS L1, L2, GLONASS,

etc.). Depending on the configuration, TRIGR can sample with a word length of up to 14-bits, at a rate of 56.32 MHz [5].

3.2.2 Antenna Array.

Figure 5. CRPA Antenna with an aluminum ground plane

The data collection was completed using the Controlled Reception Pattern Antenna (CRPA) shown in Figure 5. The shown antenna array is an ANTCOM seven element CRPA (P/N: 7NF-14CG1215P-XS-X). The array is composed of seven 3.5" diameter dual band L1/L2 GPS antennas. This configuration places a center element surrounded by six equally spaced elements on a flat surface as shown in Figure 6. The element spacing between the center element and each outer element is 11.25 cm. Note that the GPS L1 wavelength (λ_{L1}) is approximately 19.05 cm. This leads to an element spacing of $0.5906\lambda_{L1}$ for the CRPA described above.

Traditionally, the CRPA antenna is used for null forming, an antenna array technique which places a null in the direction of an interference/multipath source. However, correlator beamforming attempts to direct the beam of an antenna array at the source of the desired signal (a satellite in the case of GPS).

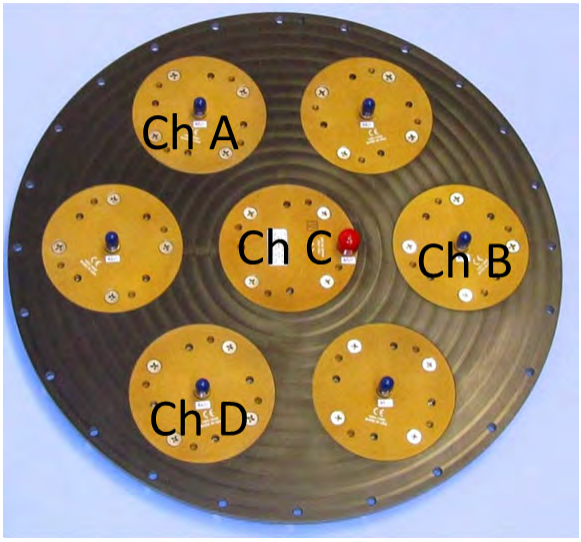

Figure 6. Element Configuration of CRPA Antenna (Figure provided by [1])

3.2.3 Data Collection.

For the purpose of this effort, the TRIGR was configured to collect four channels of L1 data simultaneously. Each channel was connected to one element of the CRPA as shown in Figure 6, with the channel D element oriented due south of the center element (channel C).

Two separate data collections were performed on 14 Jun 2013. The first was at 16:23 GMT and the second was at 19:37 GMT. Two separate data collection times where chosen in order to observe two different satellite geometries. The PRNs visible during each collection and their respective elevations are shown in Figure 7.

3.2.4 Data Downconversion.

Due to the high sample rate of the TRIGR, each data collection was downsampled to reduce processing time. The original TRIGR data had a sample frequency of $f_{s0} = 56.32$ MHz and carrier frequency $f_B = 13.68$ MHz. The desired sample rate was chosen to be 1/4 of the current sample rate which results in a new sample frequency

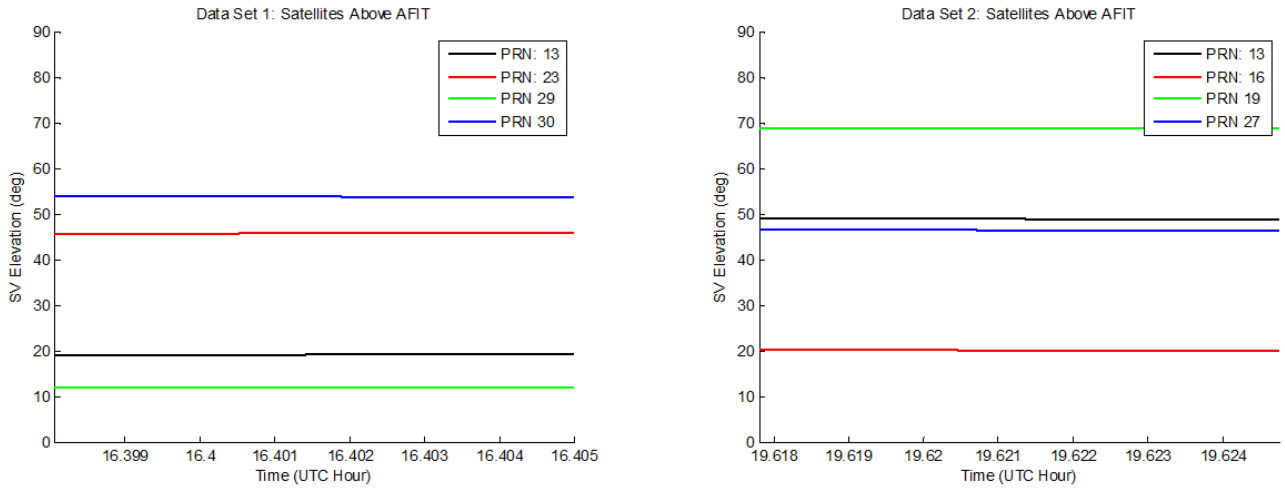

Figure 7. Elevation of Satellites Above AFIT for Data Set 1 (left) and Data Set 2 (right)

$f_s = f_{s0}/4 = 14.08$ MHz and intermediate frequency $f_{IF} = f_B/4 = 3.20$ MHz. This conversion was performed with a simple mixing and filtering operation. The following example illustrates the mixing of an arbitrary signal, $I(t) = Acos(2\pi f_B t)$

$$S(t) = I(t)cos(2\pi(f_B - f_{IF})t) \tag{7}$$

$$S(t) = Acos(2\pi f_B t)cos(2\pi(f_B - f_{IF})t) \tag{8}$$

$$S(t) = \frac{1}{2}Acos(2\pi(2f_B - f_{IF})t) + \frac{1}{2}Acos(2\pi f_{IF}t) \tag{9}$$

where $S(t)$ is the mixed signal, $cos(2\pi(f_B - f_{IF})t)$ is the mixing signal, f_B is the carrier frequency of the original signal, and f_{IF} is the desired carrier frequency of the downsampled signal.

Next, a bandpass filter, centered at f_{IF}, was used to isolate the desired signal in Equation (9). This reduced the mixed signal to

$$S_d(t) = \frac{1}{2}Acos(2\pi f_{IF}t) \tag{10}$$

which only contains the portion of the signal at f_{IF}.

Finally, the remaining signal, $S_d(t)$, was downsampled by a factor of four such that the new sample frequency is four times slower than the original sample frequency. This downsampling greatly reduced the computational burden of processing the collected data.

3.2.5 Data Switching.

In order to simulate a switched antenna, the four synchronized data sets were sampled. The switched data remained on the center channel for 0.25 seconds prior to beginning switching to allow for GPS signal acquisition. Note that signal acquisition can be performed with switched data, but this requires a beam sweeping algorithm as well (assuming that the signal's angle of arrival is unknown).

Following the 0.25 second dwell time on the center channel, the data began switching to the other elements. The dwell time on each element was set to PIT/N, where PIT is the integration period and N is the number of elements in the array. This value was chosen to ensure that each antenna element was represented during the integration period.

In addition to generating a single data file, consisting of the N element switched data, an index file was created. The index file was designed to store the element number corresponding to each data sample. This results in a second file which can easily be loaded along with the GPS data during post-processing. Figure 8 shows the element index data at the time switching begins. In the case, $PIT = 0.001$ seconds and $N = 4$ elements. Notice that each element is on for approximately 0.00025 seconds (1/4 of the integration period) after the initial 0.25 second dwell on the center element.

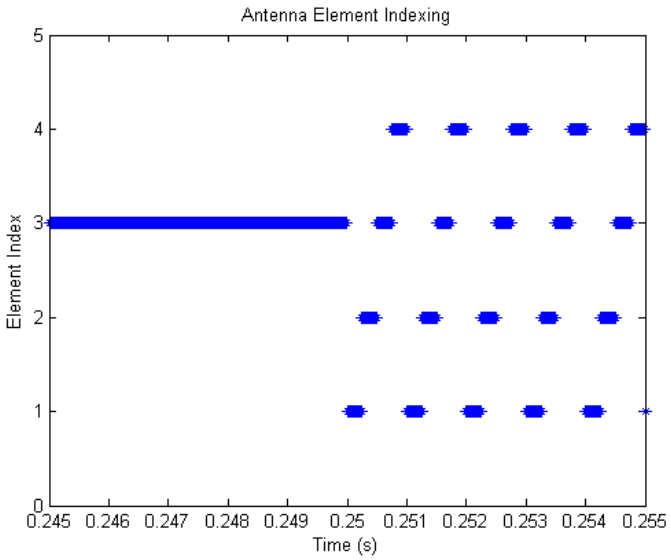

Figure 8. Antenna Index Switching: The initial dwell time on the center element was set to 0.25 **seconds to allow satellite acquisition.** $PIT = 0.001$ **seconds and** $N = 4$ **led to a dwell time of** $PIT/N = 0.00025$ **seconds on each element.**

3.3 Simulated Data Generation

Having access to simulated data enabled the testing of specific PRN and multipath configurations that are not easily obtained with real data. For example, real world data collections do not typically allow for data with a single PRN present, and a multipath signal arriving at a specific angle. This scenario allowed for the effects of multipath on pseudorange calculations to be isolated and analyzed.

3.3.1 GPS Signal Generation.

Simulated GPS signals were generated as described in [10]. This process began with specifying the antenna locations. Next, the visible PRNs were chosen along with their respective locations, carrier to noise ratio, receiver clock error (dt_{rec}), Doppler (df_{Dop}), ionosphere delay (t_{iono}), troposphere delay (t_{trop}), satellite clock error (dt_{sv}), and desired intermediate frequency (f_B). Once all the basic parameters were defined, the simulated data was generated. The process began by calculating the the code

time (t_{code})

$$t_{code} = t_{rec} - dt_{rec} - \frac{r_{true}}{c} + \frac{t_{rec} - t_{rec0}}{f_{L1}} - t_{iono} - t_{tropo} + dt_{sv} \tag{11}$$

where t_{rec} is the receiver clock, t_{rec0} is the initial receiver clock time, c is the speed of light, f_{L1} is the GPS L1 carrier frequency, and r_{true} is the distance between the satellite and antenna element. Next the carrier signal time ($t_{carrier}$) was calculated

$$t_{carrier} = t_{rec} + \frac{f_{L1}}{f_B}\left(-dt_{rec} - \frac{r_{true}}{c} + \frac{t_{rec} - t_{rec0}}{f_{L1}} - t_{iono} - t_{tropo} + dt_{sv}\right) \tag{12}$$

where f_B is the desired carrier frequency of the received signal. This value was chosen to match the intermediate frequency of the downconverted data. Finally, the I and Q data were generated using

$$I_S(t_{rec}) = A_{ca}C(t_{code})N(t_{code})cos(2\pi(f_B + df_{Dop})t_{carrier}) \tag{13}$$

$$Q_S(t_{rec}) = A_{ca}C(t_{code})N(t_{code})sin(2\pi(f_B + df_{Dop})t_{carrier}) \tag{14}$$

where A_{ca} is the signal amplitude, C is PRN's C/A Code, and N is the navigation message.

3.3.2 Noise Strength.

Assuming that the front end introduced a white Gaussian noise, the following equations allow for the simulation of the desired C/N_0 value [9]. This method assumes a noise power of 1, and defines the signal strength A_{ca} to create the desired C/N_0.

$$P_n = 1 \tag{15}$$

$$A_{ca} = \left(10^{\left(\frac{C/N_0}{10}\right)} \frac{2P_n}{f_s}\right)^{1/2} \tag{16}$$

where C/N_0 is the desired carrier to noise ratio (dB-Hz) and f_s is the sample frequency. With A_{ca} properly defined for signal generation, the noise is added in with all signals.

$$I(t) = I_S(t) + w(t) \tag{17}$$

where I_S is the signal defined by Equation (13) and w is a zero-mean white Gaussian random noise process with noise strength $E[w^2(t)] = \frac{P_n}{2}$.

3.3.3 8-bit Integer Conversion.

To generate simulated data with the same characteristics as the real data, the simulated data was converted to 8-bit integers. To perform this conversion, each data vector was scaled to be within the range of 8-bit integers [-128, 127]. This process was the final step just prior to saving the data. This allowed the use of the same software receiver for both real and simulated data without additional modifications.

3.3.4 Multipath Simulation.

Multipath was included in the simulation data by defining a reflector position. The reflector also introduced an attenuation factor and phase shift term for the multipath signal. This additional multipath signal was fully defined as

$$I_{MP}(t) = A_{MP}A_{ca}C(t_{code,MP})N(t_{code,MP})cos(2\pi(f_B + df_{Dop})t_{carrier,MP} + \phi_{MP}) \tag{18}$$

$$Q_{MP}(t) = A_{MP}A_{ca}C(t_{code,MP})N(t_{code,MP})sin(2\pi(f_B + df_{Dop})t_{carrier,MP} + \phi_{MP}) \tag{19}$$

where A_{MP} is the magnitude coefficient of the multipath and ϕ_{MP} is the phase shift due to the reflection. $t_{code,MP}$ and $t_{carrier,MP}$ are defined with Equations (11)

and (12), respectively, except r_{true} now has the value of r_{MP}, the distance from the satellite to the reflector plus the distance from the reflector to the antenna element. The final signal with multipath is defined as

$$I(t) = I_S(t) + I_{MP}(t) + w(t) \tag{20}$$

where I_S is the signal defined by Equation (13), I_{MP} is the multipath signal defined by Equation (19), and w is a zero-mean white Gaussian random noise process with noise strength $E[w^2(t)] = \frac{P_n}{2}$.

It was important to define multipath in this fashion due to the use of an antenna array. For a single antenna element, a time delay can be specified instead of calculating $t_{code,MP}$. With an antenna array, the multipath range, r_{MP}, is slightly different for each antenna, which leads to a slightly different value of $t_{code,MP}$ and $t_{carrier,MP}$ for each antenna element. Most importantly, the slightly different $t_{carrier,MP}$ for each antenna element is what simulates the multipath signal arriving from a specified direction.

3.3.5 Simulated Data Switching.

The switching for the simulated data was performed in the exact same matter as with the real data. After a set of simulated data was created for each element, the data was switch, and saved to a single file. An additional file was created with the antenna element indexes.

3.4 Software Receiver

Both the real and simulated data sets were analyzed via post-processing using a software receiver written in MATLAB®. This software receiver was developed at the

ANT Center and used in previous research efforts [6]. In order to support beamforming with switched data, a few modifications were necessary.

3.4.1 Calibration and Beamforming Phase.

The first addition to the software receiver was the inclusion of look up tables for calibration and beamforming phases. These values were defined only after processing the real, single channel, data collections. This process is discussed in more detail in Chapter IV. For the simulated data, these values were more easily defined (calibration terms are zero and beamforming phases are based on the defined geometry). The beamforming phase ϕ_{BF} can be calculated by determining the path-length difference from the satellite to each antenna element

$$\phi_{BF} = \frac{1}{\lambda_{L1}} \left(r_{sv,E} - r_{sv_0} \right) \tag{21}$$

where λ_{L1} is the GPS L1 wavelength, $r_{sv,E}$ is the distance from satellite to the antenna element of interest (each element is required to have unique beamforming phase), and r_{sv_0} is the distance from the satellite to the phase center of the antenna array (typically the center element).

3.4.2 Data Switching.

The next modification was to load the antenna element index along with the switched data. The element index data was generated to correspond one-to-one with a value in the switched data. While this method requires that the receiver load twice as much data, it is a very intuitive way to track which element a data sample came from. These index values were later used with the calibration and beamforming look up tables to apply the appropriate phase shift during Doppler removal.

3.4.3 Phase Terms.

This final step in modifying the software receiver was to incorporate the calibration and beamforming phases into the tracking loops. The following formula defines the complete phase necessary for Doppler removal:

$$\phi = \phi_k - \phi_{BF} + \phi_{Cal}$$

where ϕ_k is the traditional reference carrier, ϕ_{BF} is the beamforming phase term, and ϕ_{Cal} is the antenna calibration phase term. Performing Doppler removal with this combined phase term, ϕ, incorporates both antenna calibration and beamforming into the GPS software receiver.

3.5 Low-Noise Amplifiers

One of the primary concerns of adapting correlator beamforming to GPS is the inclusion of LNAs in the design. The LNAs have the potential to introduce phase variation in the data collected from each antenna element. If the phase variation is significant, it must be characterized and accounted for in the calibration.

Preliminary phase stabilization testing was performed on two different types of LNAs. The first type of LNA tested was the Mini-Circuits ZFL-2500+ [8] shown in Figure 9. Four of these LNAs were used along with the CRPA and TRIGR to collect data. The second type of LNA tested was the Maxim Integrated MAX2669 GPS/GNSS Ultra-Low-Noise-Figure LNA Kit [7] shown in Figure 10. This set offered a more exposed LNA, they type expected to be used on a prototype antenna array. Each LNA was tested for start up phase value, phase stability over time, and phase variation due to change in ambient temperature. The results are presented in Chapter IV.

Figure 9. Mini Circuits ZFL-2500+ LNA (Figure provided by [8])

Figure 10. Maximum Integrated MAX2669 LNA Kit (Figure provided by [7])

3.6 Summary

This chapter described the steps that were necessary to collect and generate GPS data for testing a variety of scenarios. Additionally, the modifications to the receiver were covered. Chapter IV will present the results of specific scenarios created with the above methodology.

IV. Results and Analysis

4.1 Chapter Overview

This chapter will demonstrate the capability of correlator beamforming to combine the signal of several GPS antennas. This was first accomplished with real GPS data, synchronously collected on multiple antennas using the TRIGR. The results obtained with the collected data were then replicated through simulation to validate the GPS signal simulator and beamforming values. Additional simulations were developed to show that correlator beamforming can improve tracking in a multipath environment.

4.2 Antenna Calibration

Due to the varying cable lengths, unique feed on the center element, and unknown LNA properties, the TRIGR was not expected to collect phase coherent data. The first step in performing the calibration was to run the tracking loop for each element and obtain the reference carrier (ϕ_k) for each PRN and data set.

Next, the beamforming phase was calculated by determining the expected phase difference of elements A, B, and D relative to the center element, C. Using the known antenna and satellite positions, the calculation of these beamforming phases (ϕ_{BF}) was performed as follows:

$$\phi_{BF,A} = \frac{1}{\lambda_{L1}} \left(r_{sv,A} - r_{sv,C} \right) \tag{22}$$

$$\phi_{BF,B} = \frac{1}{\lambda_{L1}} \left(r_{sv,B} - r_{sv,C} \right) \tag{23}$$

$$\phi_{BF,C} = \frac{1}{\lambda_{L1}} \left(r_{sv,C} - r_{sv,C} \right) \tag{24}$$

where λ_{L1} is the wavelength of the GPS L1 signal, $r_{sv,X}$ is the path length between the

satellite and antenna element X. Note that a set of beamforming phases is necessary for each PRN of interest due to the different location of each satellite.

Any difference between the beamforming phase and reference carrier phase was accounted for as a phase calibration term. The following equations describe the calibration terms (ϕ_{Cal}):

$$\phi_{Cal,A} = \phi_{k,A} - \phi_{k,C} + \phi_{BF,A} \tag{25}$$

$$\phi_{Cal,B} = \phi_{k,B} - \phi_{k,C} + \phi_{BF,B} \tag{26}$$

$$\phi_{Cal,D} = \phi_{k,D} - \phi_{k,C} + \phi_{BF,C} \tag{27}$$

where $\phi_{k,X}$ is the reference carrier phase for channel X, and ϕ_{BF} is the expected phase difference based on satellite geometry (beamforming phase). Note that a half cycle must be accounted for if the received signal was inverted. This occurs when the tracking loop locks onto the negative correlation of the C/A Code, and causes a phase shift of 180 degrees relative to the true phase. Table 1 shows the resulting phase terms for the first data set.

Table 1. Data Set 1 Calibration

	$\phi_{Cal,A}$ (cycles)	$\phi_{Cal,B}$ (cycles)	$\phi_{Cal,D}$ (cycles)
PRN 13	-0.2139	0.4087	-0.0680
PRN 23	-0.3784	0.4476	-0.1180
PRN 29	-0.1546	0.6585	0.1600
PRN 30	-0.3103	0.4652	-0.0705

The same technique was used to calculated the calibration terms for data set 2. The results are shown in Table 2.

The calibrations terms do vary significantly for each antenna element. In a perfect world, each value for $\phi_{Cal,A}$ would be equal. The same could be said for $\phi_{Cal,C}$ and

Table 2. Data Set 2 Calibration

	$\phi_{Cal,A}$ (cycles)	$\phi_{Cal,B}$ (cycles)	$\phi_{Cal,D}$ (cycles)
PRN 13	-0.2971	0.3992	0.0534
PRN 16	-0.1819	0.6263	0.0812
PRN 19	-0.3363	0.4921	-0.0039
PRN 27	-0.5016	0.2797	-0.1020

$\phi_{Cal,D}$. These differences are likely due to phase center variation of the patch antennas, and may be a function of satellite position as described in [2]. For the purpose of this thesis, each antenna element/PRN combination used a different calibration term.

The statistics for the phase calibrations across both data sets are shown in Table 3. The phase variation appears have a standard deviation of slightly greater than one tenth of a cycle. This result is slightly more severe than the standard deviation of approximately 0.04 cycles described in [2].

Table 3. Combined Calibration Statistics for Data Set 1 and 2

	$\phi_{Cal,A}$ (cycles)	$\phi_{Cal,B}$ (cycles)	$\phi_{Cal,D}$ (cycles)
Mean	-0.2968	0.4722	-0.0085
Standard Deviation	0.1138	0.1230	0.0989

4.3 Collected Data Results

The real GPS data consisted of four time-synchronized data collections. This collection was performed with four TRIGR RF fronts ends, set to collect GPS L1 signals. There was one data channel for each element in the antenna array. For the first data set, four PRNs (PRN: 13, 23, 29, and 30) were tracked on each of the four elements. After the individual channel results were used to calculate the calibration phases as described in the previous section, the four channels of data were combined into a single channel by simulating switching. The single channel of switched data

was then successfully processed with the software receiver by incorporating both the calibration and beamforming phases. The carrier to noise ratio for all channels and the switched data are shown for each PRN in Figure 11.

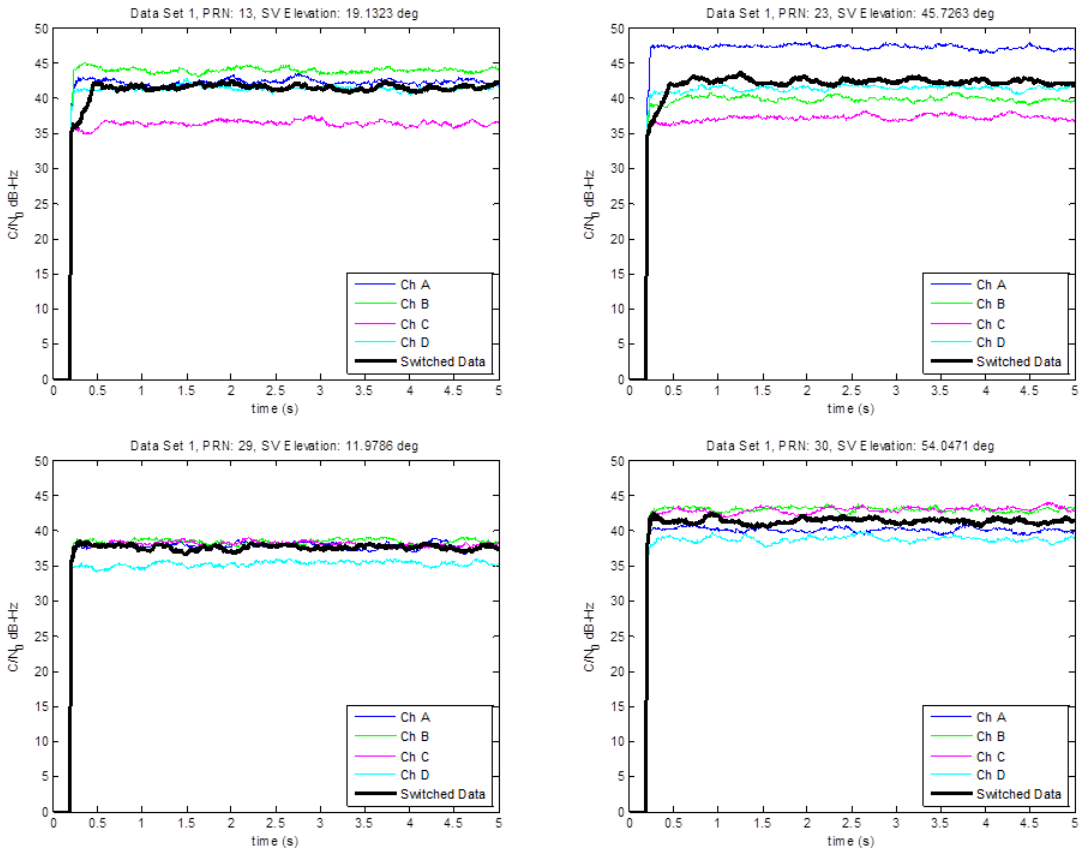

Figure 11. Data Set 1 C/N_0 vs. time

The mean carrier to noise ratio was calculated for the channel by taking the average C/N_0 over the last 3.5 seconds of each run. Additionally, the mean C/N_0 was calculated across the four channels to provide an estimate of switched data carrier to noise ratio. An additional run was completed using the average calibration phase (instead of a separate calibration for each PRN). The results are shown in Table 4.

Overall, the results of the switched data look very promising. The average C/N_0 for the switched data is always greater than or equal to the mean value across the four channels. As shown in Table 4, the results are consistently lower that of the original

Table 4. Data Set 1 C/N_0 Averaged Over 3.5 Seconds

	PRN 13	PRN 23	PRN 29	PRN 30
Ch A C/N_0 (dB-Hz)	41.88	46.86	37.67	39.73
Ch B C/N_0 (dB-Hz)	44.12	39.60	38.35	43.26
Ch C C/N_0 (dB-Hz)	36.66	36.63	38.24	42.77
Ch D C/N_0 (dB-Hz)	41.75	41.98	35.24	38.90
Mean C/N_0 Across Channels (dB-Hz)	41.10	41.27	37.37	41.17
Switched C/N_0 (dB-Hz)	42.26	42.04	37.37	41.37
Switched (Mean Cal) C/N_0 (dB-Hz)	41.22	41.88	36.12	41.31

switched data. This is to be expected since the antenna beam would be slightly off of the direct signal. The main lobe of this four element antenna is rather wide (41.68 degree half power beam width), so the loss due to using the average calibration was not too extreme (maximum loss of 1.25 dB-Hz) in this case. However, a larger antenna array with narrower beams, would be much more susceptible to calibration errors.

The second data set was analyzed in the same fashion. The results are shown in Figure 12 and Table 5. Overall, the trends are very similar to those found in data set 1, and reinforce all previously conclusions made. The switched data consistently performed slightly better than the average channel, and using the mean calibration performed slightly worse than the full calibration.

Table 5. Data Set 2 C/N_0 Averaged Over 3.5 Seconds

	PRN 13	PRN 16	PRN 19	PRN 27
Ch A C/N_0 (dB-Hz)	46.47	41.67	44.03	43.23
Ch B C/N_0 (dB-Hz)	40.17	38.00	45.13	48.33
Ch C C/N_0 (dB-Hz)	41.35	36.18	44.61	44.84
Ch D C/N_0 (dB-Hz)	37.79	39.03	41.35	40.82
Mean C/N_0 Across Channels (dB-Hz)	41.44	38.72	43.78	44.31
Switched C/N_0 (dB-Hz)	41.71	39.28	44.31	45.06
Switched (Mean Cal) C/N_0 (dB-Hz)	41.35	38.82	44.06	44.07

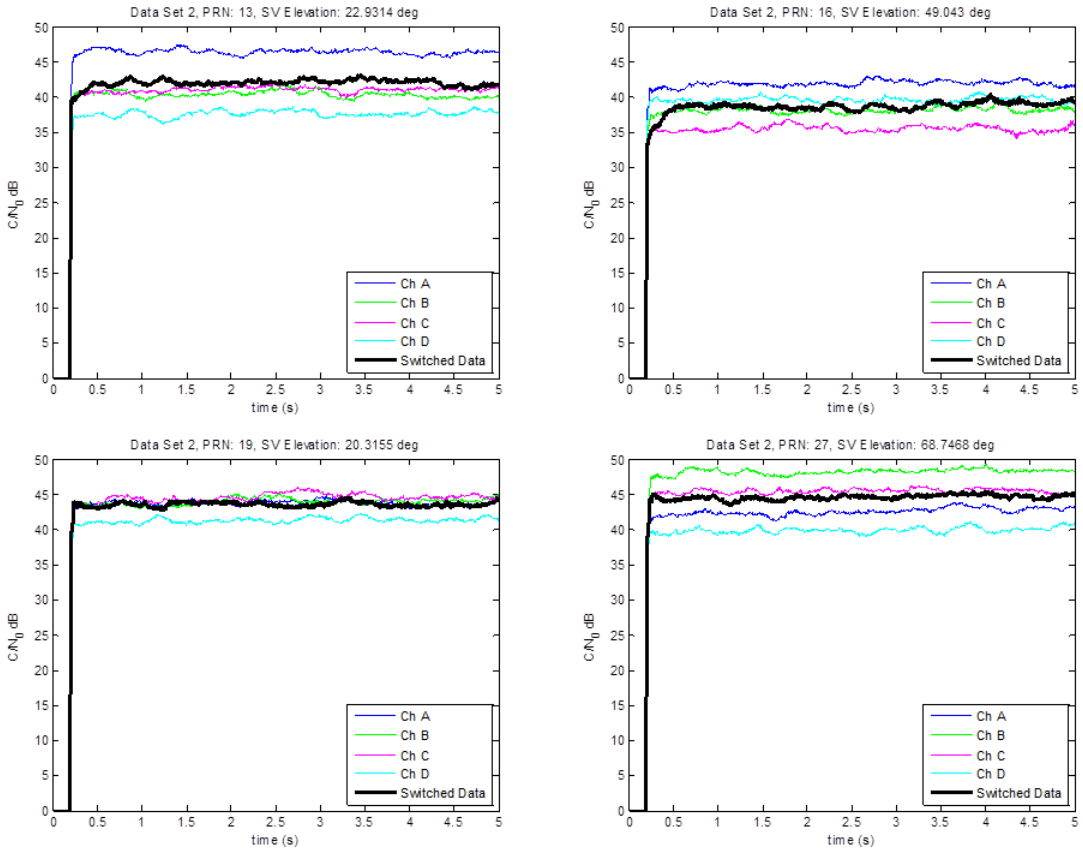

Figure 12. Data Set 2 C/N_0 vs. time

4.4 Simulation Results

The simulated data provided a lot of versatility for testing a variety of situations. Before testing more advanced scenarios, it was necessary to validate the data generation. This began with generating data sets with specific C/N_0 values. Ultimately, the satellite geometry and noise levels were chosen to closely mimic the data collections from the previous section.

4.4.1 Data Set 1 Simulation.

After generating data with the same satellite geometry and C/N_0 values of data set 1, the simulated data was switched to reproduce the results obtained in the previous section. The results are shown in Figure 13 and Table 6.

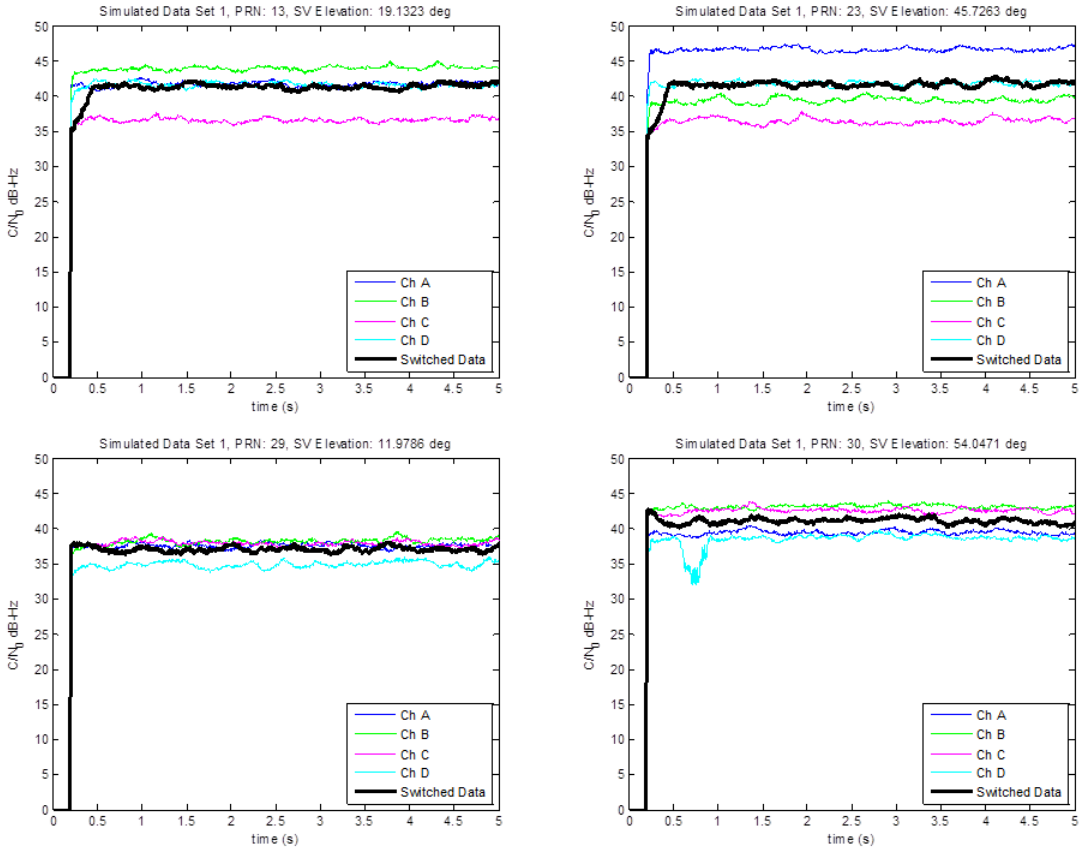

Figure 13. Simulated Data Set 1 C/N_0 vs. time

Table 6. Simulated Data Set 1 C/N_0 Averaged Over 3.5 Seconds

	PRN 13	PRN 23	PRN 29	PRN 30
Ch A C/N_0 (dB-Hz)	41.72	47.09	37.46	39.29
Ch B C/N_0 (dB-Hz)	44.06	39.80	38.95	43.29
Ch C C/N_0 (dB-Hz)	36.74	36.75	38.38	42.20
Ch D C/N_0 (dB-Hz)	41.62	41.71	35.28	38.61
Mean C/N_0 Across Channels (dB-Hz)	41.03	41.34	37.52	40.85
Switched C/N_0 (dB-Hz)	41.95	42.01	37.57	40.92

Note that the simulated data does not contain multipath, as would be expected in the real data of the previous section. However, by comparing the results of this section to Figure 11 and Table 4, it is clear that the GPS signal simulator is producing results closely mimicking those of real data.

The results of the simulated data sets also confirm the calculated beamforming phases used with the real data. In the previous section, the calibration factor could have inadvertently compensated for any errors in the beamforming phase. The simulated data did not require a calibration phase ($\phi_{Cal} = 0$), but the same beamforming phases were used for both the real and simulated GPS data. This subsequently validated the calculated beamforming phases.

4.4.2 Data Set 2.

The same process of generating simulated data was performed for data set 2. The results are shown in Figure 14 and Table 7, and closely match those of the real GPS data (see Figure 12 and Table 5). Having further validated the GPS signal simulator, other switched beamforming experiments could be performed.

4.5 4 Element Beamform Simulation

This section considers the four element antenna array used in previous sections, and analyzes a beam directed straight up, orthogonal to the plane of the array. To

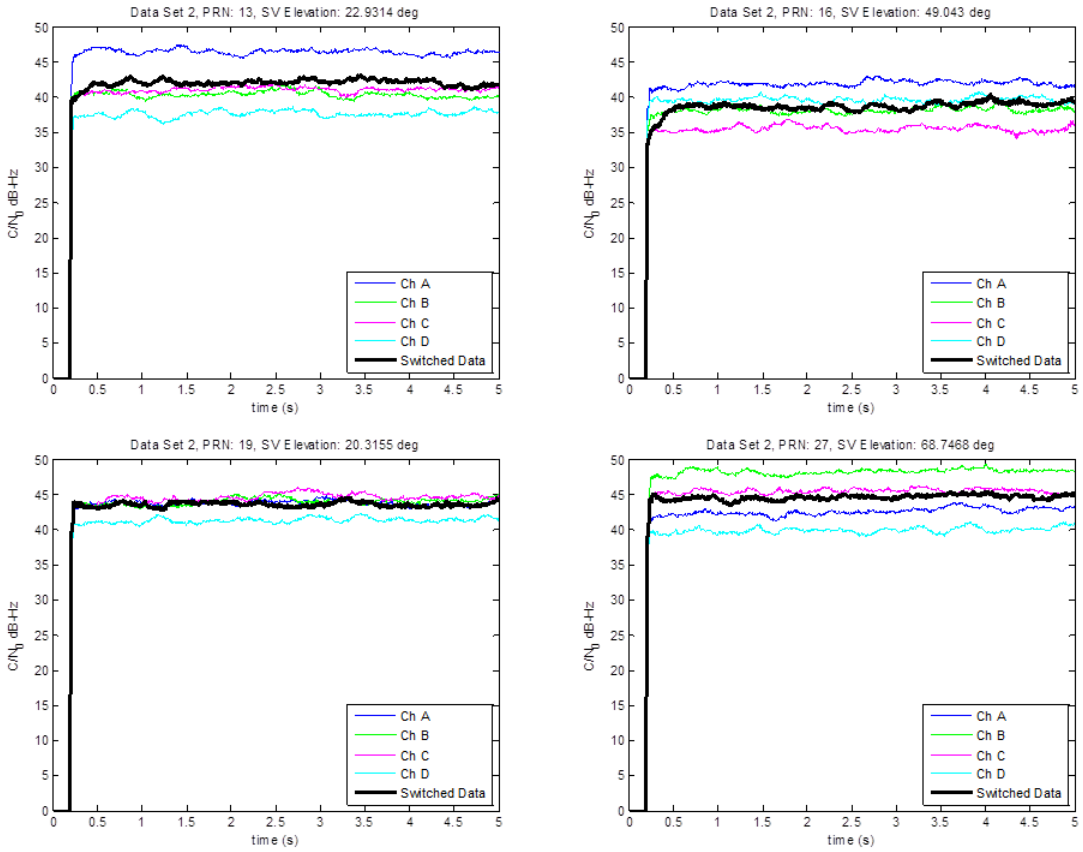

Figure 14. Simulated Data Set 2 C/N_0 vs. time

Table 7. Simulated Data Set 2 C/N_0 Averaged Over 3.5 Seconds

	PRN 13	PRN 16	PRN 19	PRN 27
Ch A C/N_0 (dB-Hz)	47.18	41.09	43.88	42.66
Ch B C/N_0 (dB-Hz)	39.87	37.29	44.68	47.69
Ch C C/N_0 (dB-Hz)	41.11	35.68	45.02	44.24
Ch D C/N_0 (dB-Hz)	37.82	39.11	41.57	40.42
Mean C/N_0 Across Channels (dB-Hz)	41.50	38.29	43.79	43.75
Switched C/N_0 (dB-Hz)	41.57	38.80	43.99	44.11

validate that a switched antenna array was capable of creating an antenna beam, a satellite was simulated at various locations over the antenna array.

First, a set of data was created for a single satellite at the horizon (0 degrees elevation), due north of the antenna. Next, the elevation was slightly increased and another data set was created. This process was repeated until data had been generated for the satellite passing directly overhead, and all the way down to the horizon, due south. At conclusion, 158 data sets were generated for this simulation.

Next, each of the 158 sets of data were switched, so that 158 single channel switched data files were created. The switched data sets were then processed using switched beamforming, with a fixed beam directed up, orthogonal to the antenna array. After each data set was processed, the average carrier to noise ratio was saved. Figure 15 shows the theoretical array factor (power) plotted with the scaled C/N_0 results. For this plot, it was necessary to convert C/N_0 from $dB \cdot Hz$ to Hz.

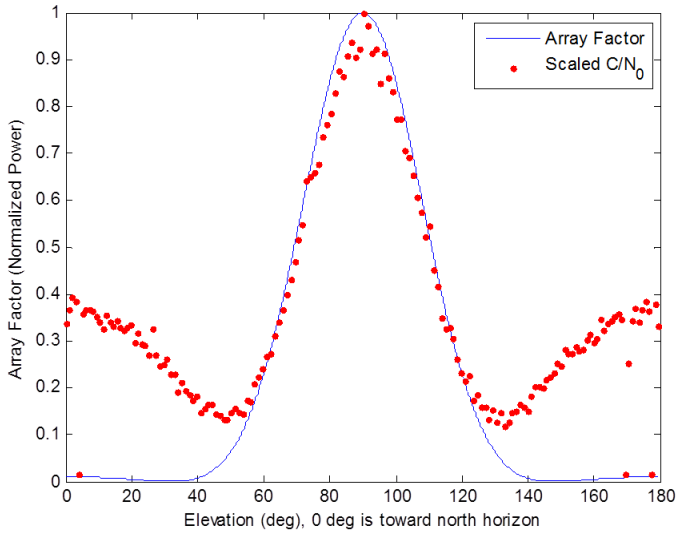

Figure 15. Four element antenna array factor (power) is shown along with the scaled C/N_0 for a single satellite passing directly over the antenna array. Elevation of 0 degrees is due north and 180 degrees is due south.

The shape of the main lobe matches closely. However, the sidelobes seem to be receiving a much higher signal power than expected. The sidelobe power is low enough

that it should be expected to stop tracking. The simulated signal had a carrier to noise ratio of 45 dB-Hz. Perhaps, if this signal was set slightly lower, the GPS receiver could not track on the side lobes. With the element spacing being greater than half a wavelength, higher sidelobes are expected. However, that was accounted for in the theoretical array factor. Overall, these results support that a beam is being properly created using correlator beamforming, but more simulations and analysis would be necessary to exactly narrow down the cause of the high C/N_0 on the sidelobes.

To further demonstrate the capability of correlator beamforming, a low elevation (0 degree) and 45 degree elevation beams were created. The results are displayed in Figure 16.

Similar to the results with the upward directed beam, the C/N_0 values closely track the main lobe, but the side lobes are higher than expected.

4.6 19 Element Beamform Simulation

This section considers a 19 element antenna array with a beam directed up, orthogonal to the antenna array. The geometry of the nineteen elements is shown in Figure 17. Adjacent elements are spaced $\lambda_{L1}/2$ apart.

Similar to the 4-element beamform analysis, 158 sets of data were generated to simulate a single satellite passing directly over the antenna array, beginning at the horizon, due north, and ending at the horizon, due south. Each set of data contained the single channel signal for 19 elements, which was used to create the switched data file. The results of the simulation are shown in Figure 18.

These results closely represent what should expected when attempting to fit carrier to noise ratio to an array factor. Not only is the main lobe followed closely by the C/N_0 data, but the GPS receiver failed to track the satellite down on side lobes, where significant losses were expected. The C/N_0 value was set to 45 dB-Hz, just as

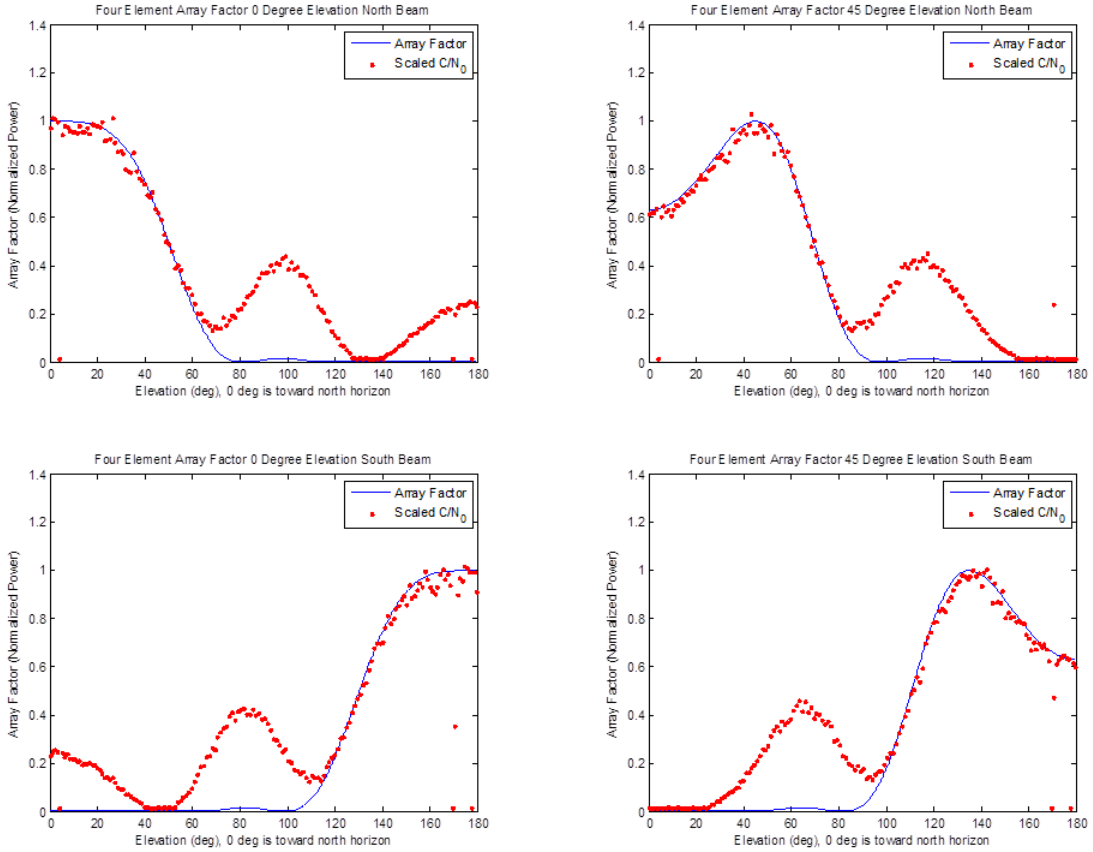

Figure 16. Four element antenna array factor (power) is shown along with the scaled C/N_0 for a single satellite passing directly over the antenna array. Elevation of 0 degrees is due north and 180 degrees is due south. Four different beams were created: 0 degrees elevation toward north (top-left), 45 degrees elevation toward north (top-right), 0 degrees elevation toward south (bottom-left), and 45 degrees elevation toward south (bottom-left).

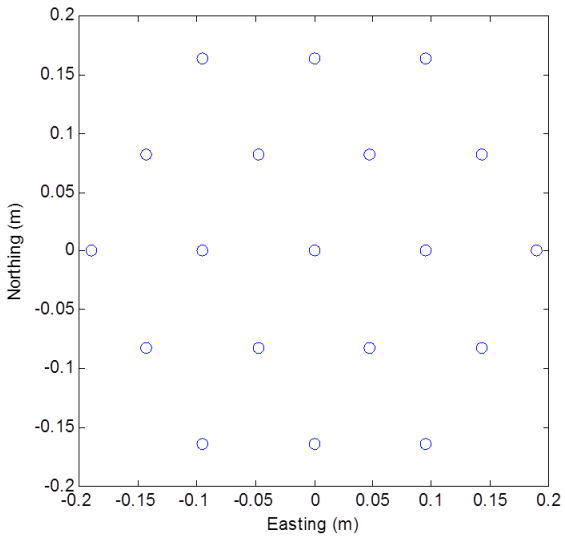

Figure 17. Nineteen Element Antenna Array Footprint

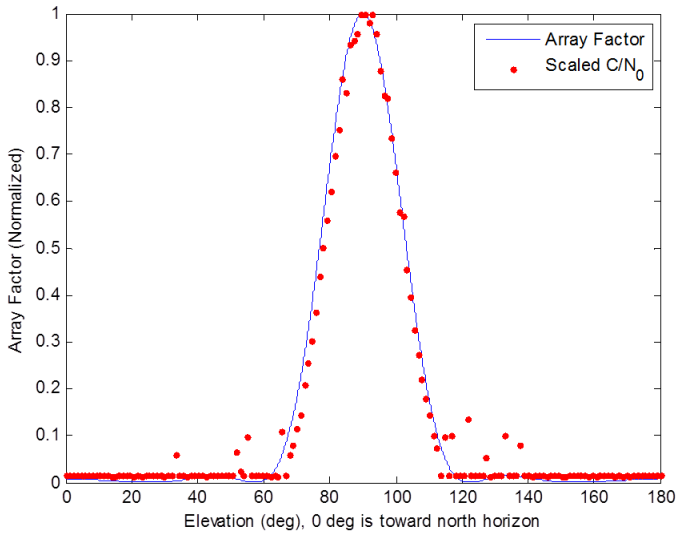

Figure 18. Ninteen element antenna array factor (power) is shown along with the scaled C/N_0 for a single satellite passing directly over the antenna array. Elevation of 0 degrees is due north and 180 degrees is due south.

it was for the four element array. There are a few stray points on the first sidelobes (near the beam) that show a slightly increased carrier to noise ratio. Overall, these results demonstrate that correlator beamforming could have applications to large GPS antenna arrays.

To further demonstrate the capability of correlator beamforming, a low elevation (0 degree) and 45 degree elevation beams were created. The results are displayed in Figure 19.

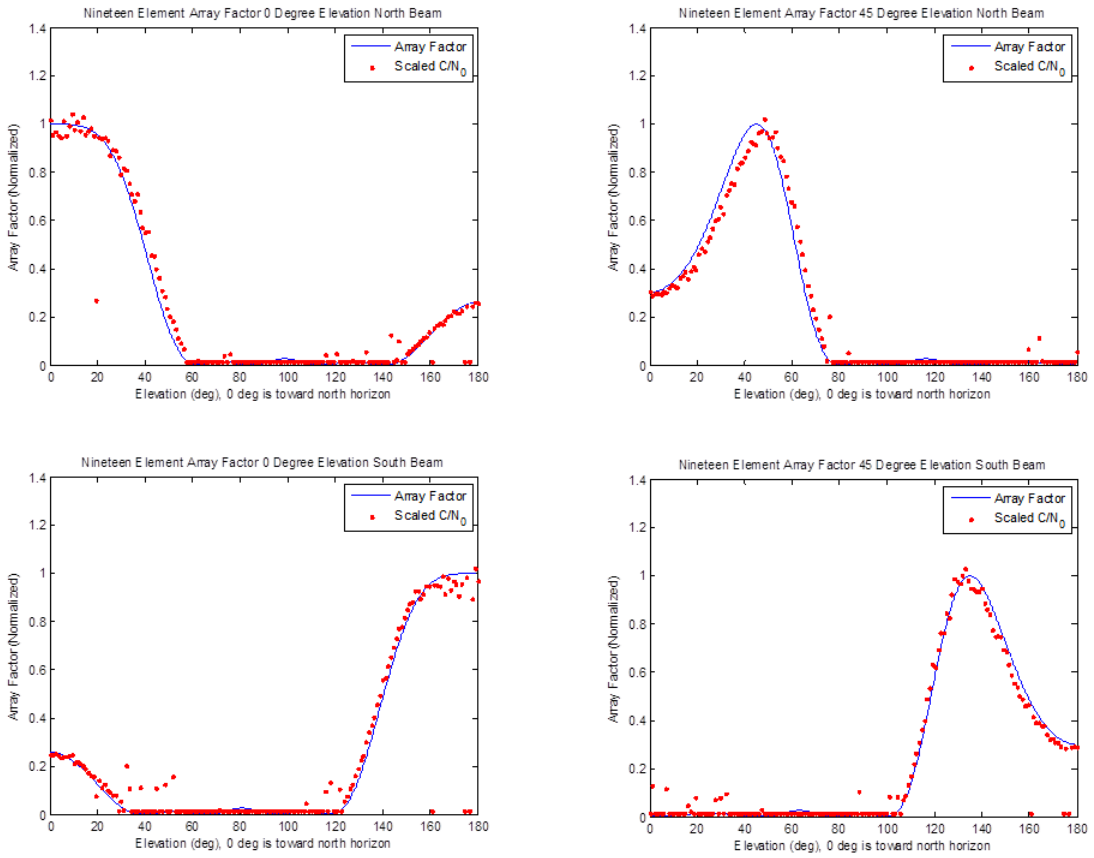

Figure 19. Nineteen element antenna array factor (power) is shown along with the scaled C/N_0 for a single satellite passing directly over the antenna array. Elevation of 0 degrees is due north and 180 degrees is due south. Four different beams were created: 0 degrees elevation toward north (top-left), 45 degrees elevation toward north (top-right), 0 degrees elevation toward south (bottom-left), and 45 degrees elevation toward south (bottom-left).

Similar to the results with the upward directed beam, the C/N_0 values closely track the main lobe, and the sidelobes are low.

4.7 Multipath Results

Having developed and tested the capability to generate GPS switched antenna data, the next logical step was to test multipath scenarios.

For the multipath simulations in the following subsections, the simulated data contains a single PRN, PRN No. 6, located directly overhead above the antenna array. The C/N_0 for each multipath scenario was set to 55 dB-Hz, a rather strong signal. This signal strength was chosen to ensure a strong lock for the baseline (no multipath) data. In this configuration, the beamforming phase terms were be set to zero, which directs the beam orthogonal to the planar array, up towards PRN 6.

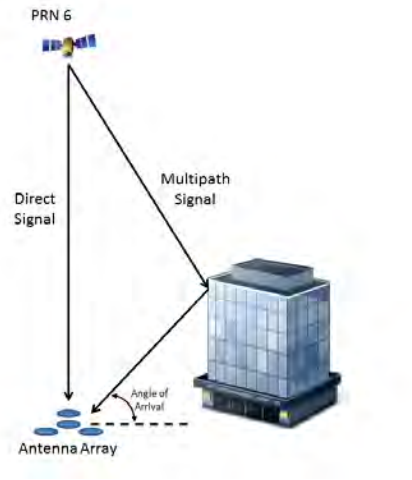

Figure 20. Multipath Diagram

4.7.1 Four Element Antenna Array, Multipath AOR at Null.

For this section, a four element antenna array is used. The center element is surrounded by three equally spaced elements, each 11.25 cm away from the center element. The array factor for the antenna, with the beam directed upward towards PRN 6, is shown in Figure 21. Note, this array factor does not include an antenna element factor.

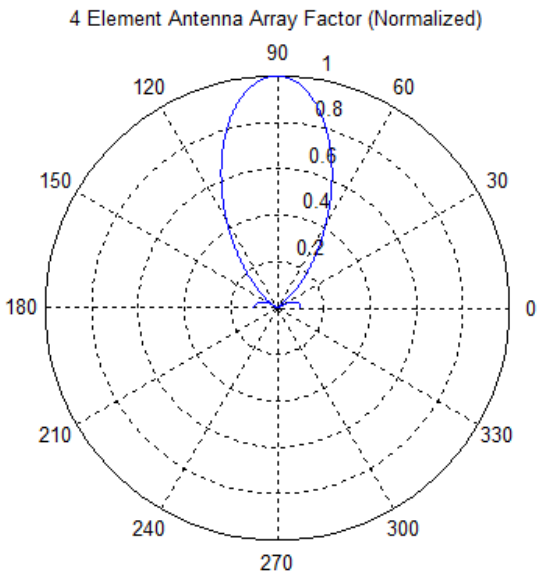

Figure 21. Four Element Antenna Array Factor as a Function of Elevation: 0 degrees elevation is due north and 180 degrees is due south.

For this set of data, a reflector (multipath source) was placed north of the antenna at an elevation of 32.15 degrees, such that the multipath's angel of arrival is on a null. The reflector was placed at a range of 10 meters. This configuration allowed for multipath rejection with beamforming, see Figure 22 . The multipath parameters were chosen to have a reflection coefficient of 0.45, 0.25 chip delay, and an applied phase shift was such that the carrier phase would be 180 degrees out of phase with the direct GPS signal at the center element.

For a single antenna receiver (center channel only), the multipath was expected to have a significant impact on the pseudorange calculation. Figure 23 shows the expected code delay of -55.68 meters for this scenario.

The center channel processing resulted in a code delay of -41.79 meters base on the average effects the multipath had on the pseudorange. The 4 element array with a beam directed at PRN 6 resulted in a delay of -16.63 meters. While this is an improvement over the single channel results, a more significant improvement was

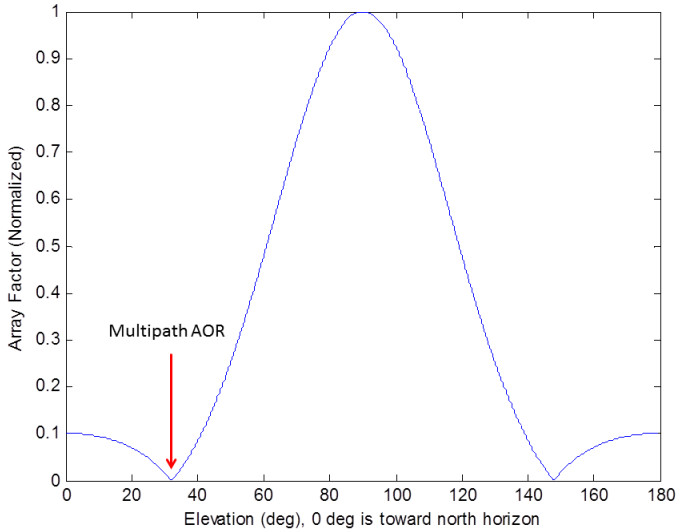

Figure 22. Four element antenna array factor is shown with a multipath angle of arrival (AOR) on the null at 32.15 degrees elevation. Elevation of 0 degrees is due north and 180 degrees is due south.

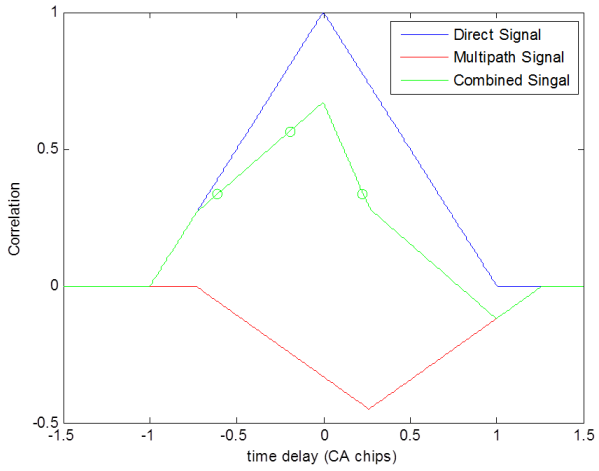

Figure 23. Four Element Multipath CA Code Correlation: The early, prompt, and late correlator's expected output are shown with the green circles. This scenario presents a potential delay of -0.19 chips.

expected (near zero delay) because the multipath was arriving on the antenna array's null.

It is worth noting the code delay was -0.09 meters for the switched antenna array with no multipath signal. This demonstrates that the switched data did not significantly impact the receiver's ability to track the GPS signal.

Another consideration of this simulation was carrier to noise ratio. The direct signal was 55 dB-Hz before the effects of multipath. The destructive multipath reduced this to 50.47 dB-Hz for the single channel antenna, while the switched antenna was able to maintain a C/N_0 of 54.68 dB-Hz. This result shows that the switched beamforming antenna was able to reject the destructive multipath because it arrived at the antenna's null.

4.8 LNA Phase Analysis

To analyze the phase stability of the LNAs the following properties were tested: start-up phase repeatability, phase stability over time, and phase variation due to change in ambient temperature. To test start-up phase repeatability, each LNA was powered on, a phase measurement was taken, and was powered off. This was repeated 10 times for each LNA. Phase stability over time was assessed by letting each LNA run continuously for three minutes following the conclusion of the start-up testing. Last, phase variation due to temperature change was assessed by heating the LNA with a hot air gun and then allowing the LNA to cool for three minutes. The results for the Mini-Circuits ZFL-2500+ LNAs are shown in Table 8.

For the purpose of correlator beamforming, these preliminary results look promising. Each start up phase value for each LNA is similar. The largest difference is between Kit A and B, a difference of 2.4 degrees. Since the start up and steady state values appear to be repeatable, a fixed calibration could account for the phase

Table 8. Mini-Circuits ZFL-2500+ LNA Phase Variation

	Kit A	Kit B	Kit C	Kit D
Start Up Phase (deg)	-119.2±0.2	-121.6±0.2	-120.8±0.2	-120.2±0.2
Steady State Phase (deg)	-119.2±0.2	-121.6±0.2	-120.8±0.2	-120.2±0.2
Under Hot Air Phase (deg)	-120.1±0.2	-122.4±0.2	-121.6±0.2	-121.4±0.2
Remove Hot Air Phase (deg)	-120.1±0.2	-122.4±0.2	-121.6±0.2	-121.4±0.2

differences between LNAs when using a real time system. The ability to quantify the relationship between temperature and phase shift was limited by not having an accurate way to measure the LNAs temperature. However, the LNAs were significantly heated by the hot air gun, the enclosures were hot to the touch. This was able to provide the type of temperature variation that might be expected while operating the LNAs outdoors, and the phase shift only changed by approximately 1 degree. Additionally, each LNA trended with temperature in a similar fashion. Since correlator beamforming is primarily concerned with phase differences relative between antenna elements, each LNA trending together would not have an affect on beamforming.

With the Mini-Circuits ZFL-2500+ LNAs the phase value did not change after 3 minutes of the hot air gun being removed. This is attributed to the metal enclosure of each LNA retaining heat. Following all tests on the final LNA, a cold pack was placed underneath the LNA to bring the temperature down. Once the LNA cooled, the phase returned to the original value of -120.2 degrees and proceeded to -119.3 degrees as the LNA continued to cool.

The results for the Maxim Integrated MAX2669 LNAs are shown in Table 9. The

Table 9. Maxim Integrated MAX2669 LNA Phase Variation

	Kit A	Kit B	Kit C	Kit D	Kit E
Start Up Phase (deg)	62.7±0.1	59.6±0.1	59.8±0.1	61.3±0.1	62.3±0.1
Steady State Phase (deg)	62.7±0.1	59.6±0.1	59.8±0.1	61.3±0.1	62.3±0.1
Under Hot Air Phase (deg)	61.8±0.1	58.4±0.1	58.4±0.1	60.2±0.1	61.4±0.1
Remove Hot Air Phase (deg)	62.7±0.1	59.6±0.1	59.8±0.1	61.3±0.1	62.3±0.1

results of testing the MAX2669 LNAs show similar results to the previous ZFL-2500+ LNAs. The start up and steady-state value are approximately constant. The largest difference between two LNAs is between Kit A and B with a phase difference of 3.1 degrees. Again this value appears to be constant during normal operation, and should be able to be accounted for with calibration. With the hot air applied, each LNA showed a change in phase shift of approximately -0.9 degrees, again showing similar behavior for each LNA. Once the hot air was removed from each LNA, the phase value started returning toward the steady-state phase value. Over the course of three minutes, each LNA had cooled and returned to the steady-state phase value. Since the MAX2669 LNA Kit is open, the LNA was able to quickly cool back to it's original operating temperature after being heated (compared to the enclosed ZFL-2500+ LNAs).

Overall, with only several degrees of relative phase difference between LNAs and the phase apparently trending together with temperature, LNAs are not expected to present a significant challenge to building a GPS antenna array for correlator beamforming.

4.9 Summary

This section presented the results of collected GPS data that was switched to simulate a switched antenna array. Simulation data was validated and used to analyze the beams of antenna arrays. The four element antenna array was then subjected to a multipath signal. The antenna array showed improved carrier to noise ratio for the multipath scenario. Improvements were also made to the signal delay, but further investigation is required. Finally, LNAs were put through preliminary testing and do not appear to pose a significant challenge for incorporation into an antenna array.

V. Conclusions and Recommendations

5.1 Conclusions of Research

Overall, significant progress was made towards creating a GPS antenna array with a single channel receiver. The feasibility of using correlator beamforming with GPS's weak signal has been verified with real world and simulated data. Additional simulations were used to explore the ability of correlator beamforming to created antenna beams in the desired direction and reject multipath arriving from obscure directions.

5.2 Significance of Research

The advantage of using this method is in the cost savings that can be achieved without the requirement for multiple channel receivers. Technically, beamforming can be performed with traditional phased antenna arrays. However, an N-element array would typically require an N-channel RF front end, which can cause cost to become impractical. With this method, only a single channel RF front end would be required, thus resulting in a potentially huge cost savings.

5.3 Recommendations for Future Research

Having successfully switched and performed beamforming with collected and simulated GPS data, the next logical step for this effort is to build the switched antenna with real hardware. Dr. Collins (committee member) and I have completed much of the design over the course of this thesis, but several issues must still be resolved.

For the physical implementation of the switched antenna, a more robust characterization of the LNAs may be necessary, depending upon the expected operating

environment and number of elements. In general, the more elements used in the array, the more narrow the resulting antenna beam will be. If very narrow beams are desired, a careful characterization and calibration of the LNAs will likely be necessary.

One of the remaining hurdles remaining is to narrow down the method of timing and controlling the antenna switching. A Complex Programmable Logic Device (CPLD) program has already been developed to control the switching. However, the Transform-Domain Instrumentation Global Navigation Satellite System Receiver (TRIRG) will have no way of distinguishing which samples belong to a particular antenna element. A variety of methods have been considered for this, but none of them have been tested enough to justify publication.

Beyond hardware implementation, the simulations presented in this thesis only scratch the surface of the options available with correlator beamforming. Additional research could focus on more elaborate multipath scenarios, adjusting element gain (in addition to phase) values, or the incorporation of null forming.

Finally, signal acquisition was not performed with switched data in this thesis. Algorithms should be developed that search spatially for GPS signals during signal acquisition. Furthermore, this could be coupled with an inertial navigation system to perform beamforming and satellite tracking for antenna arrays mounted on moving platforms (e.g. vehicles).

Bibliography

1. ANTCOM Corporation, 367 Van Ness Way, Torrance, CA 90501. *7-Element CRPA Datasheet*, April 2013. Available at *http://www.antcom.com*.

2. Backén, Staffan, Dennis M Akos, and Magnus L Nordenvaad. "Post-Processing Dynamic GNSS Antenna Array Calibration and Deterministic Beamforming". *Proceedings of the 21st International Technical Meeting of The Satellite Division of the Institute of Navigation (ION GNSS 2008)*, 2806–2814. 2008.

3. Balanis, Constantine A. *Antenna Theory*. John Wiley and Sons, Inc., Hoboken, New Jersey, 2005.

4. Barnes, J, C Rizos, M Kanli, A Pahwa, D Small, G Voigt, N Gambale, and J Lamance. "High accuracy positioning using Locatas next generation technology". *18th Int. Tech. Meeting of the Satellite Division of the US Institute of Navigation*, 2049–2056. 2005.

5. Gunawardena, Sanjeev. *Development of a Tranform-Domain Instrumentation Global Positioning System Receiver for Signal Quality and Anomalous Event Monitoring*. Ph.D. thesis, Ohio Univerisity, 2007.

6. Haker, Marshall E. *Modeling the Effects of the Local Environment on a Received GNSS Signal*. Ph.D. thesis, Air Force Institute of Technology, Wright-Patterson AFB, March 2013.

7. Maxim Integrated, 16848 Southpark Drive, Suite 500, Westfield, IN 46074. *MAX2669 Low Noise Amplifier Data Sheet*, September 2012. Available at *http://www.maximintegrated.com/*.

8. Mini-Circuits, 13 Neptune Ave, Brooklyn, NY 11235. *ZFL-2500+ Low Noise Amplifier Data Sheet*. Available at *http://http://www.minicircuits.com/*.

9. Misra, Pratap and Per Enge. *Global Positioning System Signals, Measurements, and Performance*. Ganga-Jamuna Press, Lincoln, Massachusetts, 2012.

10. Raquet, John F. "EENG 633: GPS Receiver Design". Course Notes.

11. Rizos, Chris, Yong Li, and Wei Jiang. "Locata for Indoor Positioning Using Beam-Forming Technology". International Symposium on GNSS, October 2013.

12. Zarchan, Paul and Others. *Global Positioning System: Theory and Applications Volume I*. American Institute of Aeronautics and Astronautics, Inc., Washington, DC, 1996.

REPORT DOCUMENTATION PAGE

Form Approved
OMB No. 0704–0188

1. REPORT DATE *(DD–MM–YYYY)*	2. REPORT TYPE	3. DATES COVERED *(From — To)*
14–03–2014	Master's Thesis	Aug 2012 — Mar 2014

4. TITLE AND SUBTITLE

GPS MULTIPATH REDUCTION WITH CORRELATOR BEAMFORMING

5a. CONTRACT NUMBER

5b. GRANT NUMBER

5c. PROGRAM ELEMENT NUMBER

6. AUTHOR(S)

Barhorst, Jason M. Captian, USAF

5d. PROJECT NUMBER

5e. TASK NUMBER

5f. WORK UNIT NUMBER

7. PERFORMING ORGANIZATION NAME(S) AND ADDRESS(ES)

Air Force Institute of Technology
Graduate School of Engineering and Management (AFIT/EN)
2950 Hobson Way
WPAFB OH 45433-7765

8. PERFORMING ORGANIZATION REPORT NUMBER

AFIT-ENG-14-M-10

9. SPONSORING / MONITORING AGENCY NAME(S) AND ADDRESS(ES)

Locata Corporation
3651 Lindell Road, Suite D
Las Vegas, NV 89103
COMM 702-701-1691
Email: Paul.Benshoof@locatacorp.com

10. SPONSOR/MONITOR'S ACRONYM(S)

11. SPONSOR/MONITOR'S REPORT NUMBER(S)

12. DISTRIBUTION / AVAILABILITY STATEMENT

DISTRIBUTION STATEMENT A: APPROVED FOR PUBLIC RELEASE; DISTRIBUTION UNLIMITED.

13. SUPPLEMENTARY NOTES

This material is declared a work of the U.S. Government and is not subject to copyright protection in the United States.

14. ABSTRACT

This research effort investigates the feasibility of beamforming using a single Global Positioning System (GPS) front end. Traditional methods of beamforming use multiple front ends, typically one per antenna element. By enabling a receiver to sample a switched antenna array, the hardware cost of implementing a GPS antenna array can be significantly reduced. Similar techniques of reducing the number of receivers have been used by Locata Corporation in the design of their non-GPS positioning systems. However, Locata Corporation's local transmitters provide a signal strength much higher than GPS's signal strength. For this reason, the inclusion of low-noise amplifiers into the GPS based system was investigated.

GPS data was collected using a multiple channel antenna array. Simulated switching was then performed to combine the four channels of data in to a single channel of switched data. Next, a GPS receiver using correlator beamforming was developed to apply the necessary phase shift to each data sample and form an antenna beam in the direction of the desired satellite. The switched data was processed and analyzed with the receiver. The results successfully demonstrated the potential for correlator beamforming to be used with GPS signals. Additional experiments were performed with simulated GPS data to further characterize the capability of the receiver.

15. SUBJECT TERMS

GPS, Antenna Array, Multipath, Beamforming

16. SECURITY CLASSIFICATION OF:			17. LIMITATION OF ABSTRACT	18. NUMBER OF PAGES	19a. NAME OF RESPONSIBLE PERSON
a. REPORT	b. ABSTRACT	c. THIS PAGE			Dr. John F. Raquet, AFIT/ENG
U	U	U	U	59	19b. TELEPHONE NUMBER *(include area code)* (937) 255-3636, x4580; john.raquet@afit.edu